

Plasmon-induced nonlinear response on gold nanoclusters

Yuhui Song(宋玉慧), Yifei Cao(曹逸飞), Sichen Huang(黄思晨), Kaichao Li(李凯超), Ruhai Du(杜如海), Lei Yan(严蕾), Zhengkun Fu(付正坤), and Zhenglong Zhang(张正龙)

Citation: Chin. Phys. B, 2024, 33 (**4**): 044204. DOI: 10.1088/1674-1056/ad1a8b
Journal homepage: http://cpb.iphy.ac.cn; http://iopscience.iop.org/cpb

What follows is a list of articles you may be interested in

Tunable spectral continuous shift of high-order harmonic generation in atoms by a plasmon-assisted shaping pulse

Yuan Wang(王源), Yulong Li(李玉龙), Yue Qiao(乔月), Na Gao(高娜),Fu-Ming Guo(郭福明), Zhou Chen(陈洲), Lan-Hai He(赫兰海),Yu-Jun Yang(杨玉军), Xi Zhao(赵曦), and Jun Wang(王俊)

Chin. Phys. B, 2024, 33 (**3**): 034212. DOI: 10.1088/1674-1056/ad10fb

Giant and controllable Goos—Hänchen shift of a reflective beam off a hyperbolic metasurface of polar crystals

Tian Xue(薛天), Yu-Bo Li(李宇博), Hao-Yuan Song(宋浩元), Xiang-Guang Wang(王相光), Qiang Zhang(张强), Shu-Fang Fu(付淑芳), Sheng Zhou(周胜), and Xuan-Zhang Wang(王选章)

Chin. Phys. B, 2024, 33 (**1**): 014207. DOI: 10.1088/1674-1056/acdac2

Enhanced and controllable reflected group delay based on Tamm surface plasmons with Dirac semimetals

Qiwen Zheng(郑棋文), Wenguang Lu(卢文广), Jiaqing Xu(胥加青),Yunyang Ye(叶云洋), Xinmin Zhao(赵新民), and Leyong Jiang(蒋乐勇)

Chin. Phys. B, 2023, 32 (**7**): 074208. DOI: 10.1088/1674-1056/aca205

Simultaneous measurements of refractive index and temperature based on a no-core fiber coated with Ag and PDMS films

Yuxin Li(李宇昕), Hailiang Chen(陈海良), Yingyue Zhang(张赢月), Qiang Chen(陈强), Biao Wu(武彪),Xiaoya Fan(樊晓亚), Yingchao Liu(刘英超), and Mingjian Ma(马明建)

Chin. Phys. B, 2023, 32 (**5**): 054209. DOI: 10.1088/1674-1056/ac8f36

Molecular fluorescence significantly enhanced by gold nanoparticles@zeolitic imidazolate framework-8

Yuyi Zhang(张钰伊), Yajie Bian(卞亚杰), Wei Zhang(张炜), Yiting Liu(刘易婷), Xiaolei Zhang(张晓磊),Mengdi Chen(陈梦迪), Bingwen Hu(胡炳文), and Qingyuan Jin(金庆原)

Chin. Phys. B, 2023, 32 (**5**): 054208. DOI: 10.1088/1674-1056/ac81aa

---

SPECIAL TOPIC — Optical field manipulation

Plasmon-induced nonlinear response on gold nanoclusters

Yuhui Song(宋玉慧), Yifei Cao(曹逸飞), Sichen Huang(黄思晨), Kaichao Li(李凯超), Ruhai Du(杜如海), Lei Yan(严蕾)†, Zhengkun Fu(付正坤), and Zhenglong Zhang(张正龙)‡

School of Physics and Information Technology, Shaanxi Normal University, Xi'an 710119, *China*

(Received 11 October 2023; revised manuscript received 29 December 2023; accepted manuscript online 4 January 2024)

The plasmon-induced nonlinear response has attracted great attention in micro-nano optics and optoelectronics applications, yet the underlying microscopic mechanism remains elusive. In this study, the nonlinear response of gold nanoclusters when exposed to a femtosecond laser pulse was investigated using time-dependent density functional theory. It was observed that the third-order tunneling current was augmented in plasmonic dimers, owing to a greater number of electrons in the dimer being excited from occupied to unoccupied states. These findings provide profound theoretical insights and enable the realization of accurate regulation and control of nonlinear effects induced by plasmons at the atomic level.

Keywords: plasmon, nonlinear optics, time-dependent density functional theory (TDDFT)

PACS: 42.65.–k, 31.15.ee, 36.40.Vz **DOI:** 10.1088/1674-1056/ad1a8b

Nonlinear optics, a vital component of modern optics and photonics, has widespread applications in areas such as optical harmonic generation,[1] laser frequency modulation,[2] ultrafast optical switching,[3] optical detection[4] and optical imaging.[5] The nonlinear response comes from the anharmonic correction of the potential field experienced by electrons or molecules within the material, and this contribution becomes significant only under intense optical fields.[6] For the development and application of nanoscale integrated optics, the investigation of weak light nonlinear optics at the nanoscale is particularly crucial.[7–10] Localized surface plasmon resonance (LSPR), originating from the interaction between electromagnetic waves and free electrons in metals, can greatly amplify the electromagnetic field energy density within the subwavelength spatial scale of the metal surface.[11,12] This enhancement effectively boosts the amplitude of nonlinear effects, diminishes the incident light intensity required for nonlinear processes and promotes the generation of weak light nonlinear effects in the nanoscale domain.[13–15]

Gold nanostructures are typical plasmonic materials that exhibit an excellent plasmonic response,[16] are easily synthesized[17] and have excellent biocompatibility.[18] Consequently, they have garnered immense attention. By tailoring the size and shape of gold nanostructures, fascinating phenomena can be observed.[19,20] Nonlinear effects can be significantly amplified through LSPR by altering the morphology of gold nanostructures.[21] For instance, the utilization of non-centrosymmetric gold nanocups can effectively enhance second-harmonic generation,[22] while the employment of a gold bowtie antenna can generate third-harmonic generation.[23] Although these studies have made significant contributions to the field of nonlinear plasmons, the theoretical foundations of symmetric and asymmetric gold nanoclusters still require further exploration to elucidate the microscopic mechanisms and realize accurate regulation and control of nonlinear optics at the atomic level.

In this study, we employ the time-dependent density functional theory (TDDFT)[24] to explore the real-time dynamics of the nonlinear response of Au_8 clusters and Au_8–Au_8 dimers upon irradiation by a femtosecond laser pulse. Our findings reveal that the third-order nonlinear effect is more pronounced in Au_8–Au_8 dimers than individual Au_8 clusters. This can be attributed to the fact that in Au_8–Au_8 dimers a larger number of electrons transition from occupied to unoccupied states compared with in single Au_8 clusters. This investigation provides a deeper understanding of plasmon-induced nonlinear processes.

The first-principles calculations were performed using the real-space TDDFT code OCTOPUS,[25] using the local density approximation[26] for exchange–correlation functions. The simulation domain was defined by assigning a sphere with a radius of 6.0 Å around each atom, and the electronic wave functions were represented on a uniform grid within the simulation region, with a spacing of 0.25 Å between grid points. Hartwigsen–Goedecker–Hutter[27] pseudopotentials were utilized to describe the interaction between valence electrons and the atomic core. The spectrum of light absorption and the tunneling current were obtained by propagating the electronic density for 15000 steps with a time step of 0.0026 fs following laser excitation and a Gaussian wave packet of laser pulses. The electric field is applied in the length gauge by adding the external potential in the form of $V_{\text{ext}}(\boldsymbol{r},t) = \boldsymbol{E}(t)\cdot\boldsymbol{r}$.

†Corresponding author. E-mail: yanlei@snnu.edu.cn
‡Corresponding author. E-mail: zlzhang@snnu.edu.cn

© 2024 Chinese Physical Society and IOP Publishing Ltd

We initially compared the tunneling current responses of Au_8 and Au_8–Au_8 dimers induced by the laser field depicted in Fig. 1. The geometric configurations of Au_8 and Au_8–Au_8 are respectively presented in Figs. 1(a) and 1(d). In all simulations, the Au atoms within the gold clusters were fixed after undergoing geometric relaxation. When photons interact with particulate matter, if the size of the particulate matter is comparable to the wavelength of the photon a strong resonance absorption peak will appear in the scattering spectrum, a phenomenon known as Mie resonance.[28] The absorption spectrum of Au_8 is primarily characterized by a Mie resonance at approximately 4.82 eV, while that of Au_8–Au_8 dimers is at approximately 4.85 eV, as illustrated in Fig. S1. We directly analyze the tunneling currents of Au_8 and Au_8–Au_8 dimers when exposed to ultrafast femtosecond laser pulses. We apply a Gaussian wave packet linearly polarized in the z direction along the gold cluster, $E(t) = E_{\max}\exp[-(t-t_0)^2/2\tau^2]\cos(\omega t-\omega t_0)$. Here, the pulse width τ is 3.3 fs and the frequency ω is set to the plasmon resonant energy of 4.824 eV for Au_8 (refer to Fig. 1(b)) and 4.853 eV for Au_8–Au_8 (refer to Fig. 1(e)). Both laser field intensities reach their maximum value of $E_{\max} = 0.025$ V·Å^{-1} at the time $t_0 = 10$ fs. The current I_t is collected at the central plane located 2.9 Å from the end atom of the Au_8 clusters, and at the same position for the Au_8–Au_8 dimer. In both Au_8 (Fig. 1(c)) and Au_8–Au_8 (Fig. 1(f)), the oscillation amplitude of the tunneling current continues to increase until $t = 20$ fs. In Au_8, when the field intensity reaches its maximum, the tunneling current continues to oscillate and exhibits a phase shift in its oscillation and appears with high-frequency modulation.[29] As time progresses, the high-frequency modulation becomes more prominent (Fig. 1(c)). In the Au_8–Au_8 dimer, after 20 fs field attenuation, the oscillation amplitude of the tunneling current decreases at 20–30 fs and increases at 30–40 fs (Fig. 1(f)).

In Fig. 2, we investigate the dependence of the nonlinear responses of Au_8 and Au_8–Au_8 on laser intensity. The tunneling current spectra of Au_8 (Fig. 2(a)) and Au_8–Au_8 (Fig. 2(b)) were obtained by performing a Fourier transform on their time evolution under varying laser intensities ($E_{\max} = 0.013$, 0.019 and 0.025 V·Å^{-1}). It is observed that, except for the Mie resonance, Au_8 also exhibited second-order and third-order excitations whereas the Au_8–Au_8 dimer exhibited only third-order excitation. Notably, the second peak of Au_8 is even higher than the Mie resonance. Through further analysis of the ratio of the Mie resonance and the third-order tunneling current spectra peaks of the Au_8–Au_8 dimer to Au_8 with varying laser intensities ($E_{\max} = 0.013$, 0.019 and 0.025 V·Å^{-1}), we find that the ratio of the peak value of the first-order tunneling current spectra of the Au_8–Au_8 dimer to Au_8 gradually decreases from approximately 2 as to 1 as the field intensity increases. In contrast, the ratio of the peak value of the third-order tunneling current spectra increases from approximately 1 to 2.5 with the increase in intensity. This indicates that the Au_8–Au_8 dimer exhibits a significant enhancement in third-order tunneling current compared with single Au_8 clusters as the intensity increases.

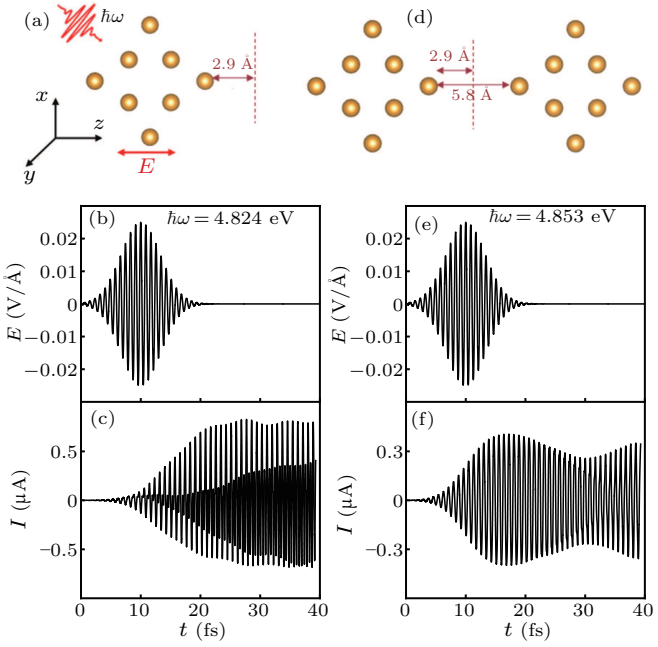


Fig. 1. Schematic diagram illustrating an Au_8 cluster (a) and an Au_8–Au_8 dimer (d) under a laser pulse polarized in the z direction. Panels (b) and (e) depict the time evolution of the corresponding laser pulse for Au_8 and Au_8–Au_8, respectively. Under the laser, the corresponding time evolution of the tunnel currents at the end of (c) Au_8 and at the center of (f) the Au_8–Au_8 dimer.

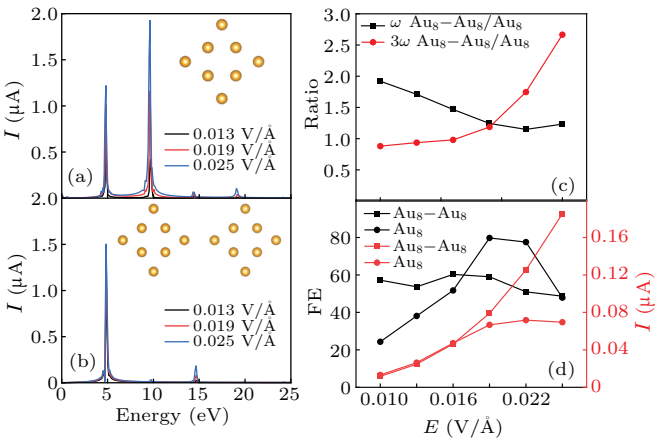


Fig. 2. Evolution of tunneling current spectrum of Au_8 (a) and Au_8–Au_8 (b), respectively, during impulse excitation with varying laser intensities ($E_{\max} = 0.013$, 0.019 and 0.025 V·Å^{-1}). (c) The ratio of the first-order (black line) and third-order (red line) tunneling current spectra of the Au_8–Au_8 dimer to that of Au_8 with different laser intensities ($E_{\max} = 0.01$, 0.013, 0.016, 0.019 and 0.025 V·Å^{-1}). (d) Field enhancement (black line) and tunneling currents (red line) as a function of varying laser intensities for Au_8 (circles) and Au_8–Au_8 (squares).

To compare the effects of dimerization on the electronic properties, the tunneling current spectrum was calculated by gradually increasing the distances between the dimer components. First, we fixed the left Au_8 and calculated the cross

section of the dimer in Fig. S2(a). Then we calculated the tunneling current spectrum of the Au_8–Au_8 dimer by increasing the distance D between the right Au_8 and the calculated cross section from 2.9 Å to 4.9 Å. With the distances increasing, especially when $D = 4.9$ Å the spectral shape of the tunneling current spectrum is similar to that of a single Au_8 cluster, and the intensities of the first and second-order peaks decrease to half that of a single Au_8 peak in Fig. S2(b). If we gradually increase the distances between the dimer components, one should gradually obtain the single nanocluster case. The occupation of Kohn–Sham (KS) states is calculated by projecting the time-dependent KS state onto the KS orbitals at time $t = 0$, which requires Au atoms to be fixed. In the calculation of the tunneling current, we still fix Au atoms for the sake of the consistency of the calculation, and we compare the tunneling current by fixing gold atoms and moving gold atoms of Au_8 and Au_8–Au_8 in Fig. S3. The tunneling current of Au_8–Au_8 is almost unaffected by whether or not Au atoms are fixed. For Au_8, if the Au atoms are moved, the peak position of the tunneling current has no movement and the peak strength shows a certain change compared with that of fixed Au atoms. Importantly, the enhancement of the third-order tunneling current of Au_8–Au_8 compared with that of Au_8 is not affected by whether or not the gold atoms are fixed. Therefore, we chose to fix the coordinates of the gold atoms for all simulations.

To gain a deeper understanding of the tunneling current response, we present the peak values of tunneling current spectra and field enhancement measured at a central plane located 2.9 Å from the atom at the end of the Au_8 cluster and at the same position for the Au_8–Au_8 dimer. These peak values are shown under different laser intensities ranging from $E_{max} = 0.01$ V·Å^{-1} to 0.025 V·Å^{-1} in Fig. 2(d). It is observed that the tunneling current of Au_8 increases with the laser intensity; nevertheless, its field enhancement initially increases and then decreases, exhibiting an inverse correlation with the tunneling current.[30] The field enhancement between the nanoparticle dimer is weakened because an interparticle current resulting from the strong field photoemission tends to neutralize the plasmon-induced surface charge density.[14] This conclusion is consistent with our result that the field enhancement for the dimer is smaller compared to that for the single cluster under higher intensity. On the other hand, the tunneling current of the Au_8–Au_8 dimer increases with the laser intensity; however, its field enhancement trend remains within a certain range and is not consistently correlated with laser intensity. Therefore, for both Au_8 and Au_8–Au_8 there is no significant correlation between the tunneling current and the field enhancement. Based on these observations, we can infer that field enhancement does not play a significant role in the nonlinear response induced by plasmonic excitation of gold nanoclusters.

To further elucidate the phenomenon wherein the third-order tunneling current of the Au_8–Au_8 dimer is approximately 2.5 times stronger than that of Au_8 under the field $E_{max} = 0.025$ V·Å^{-1}, we present the time-dependent changes in the occupation of the KS states for Au_8 and Au_8–Au_8 under the same field strength in Fig. 3. The occupation of KS states is calculated by projecting the time-dependent KS state onto the KS orbitals at time $t = 0$. The population inversion of the electrons from deep-energy to high-energy states is usually the result of the nonradiative decay of plasmons into hot electrons.[31,32] By comparing Figs. 3(a) and 3(b), it can be observed that the number of electron transitions from all occupied states to unoccupied states in the Au_8–Au_8 dimer is greater than that in single Au_8 clusters. Based on these findings, we can infer that the atomic mechanism behind the enhanced third-order tunneling current of Au_8–Au_8 is due to the varied contributions of hot electrons generated by plasmon decay to the occupation number of KS orbitals. This, in turn, affects the nonlinear response.

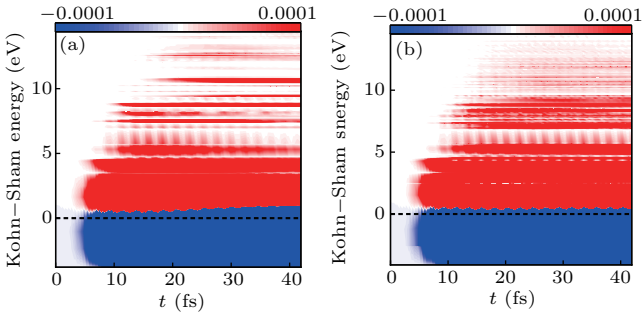


Fig. 3. Time-dependent changes in the occupation of the Kohn–Sham states for (a) Au_8 and (b) Au_8–Au_8 under the field $E_{max} = 0.025$ V·Å^{-1}. The energy zero denotes the Fermi level.

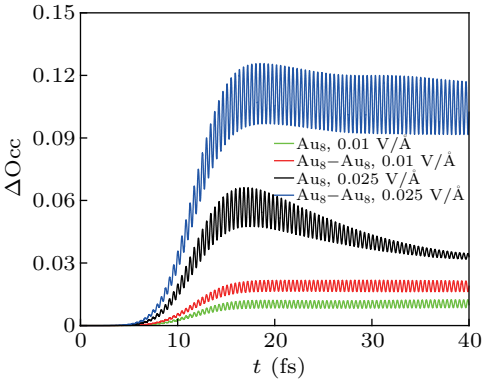


Fig. 4. Time evolution of the transition number from occupied states to unoccupied states of Au_8 and Au_8–Au_8 under the field strengths $E_{max} = 0.01$ V·Å^{-1} and 0.025 V·Å^{-1}.

The analysis of the number of electron transitions from all occupied states to the unoccupied states for Au_8 and Au_8–Au_8 under fields $E_{max} = 0.01$ V·Å^{-1} and 0.025 V·Å^{-1}, presented in Fig. 4, further confirms the above conclusion. It is found that the number of electron transitions from all occupied states to unoccupied states in Au_8–Au_8 is greater than that in Au_8 under the same field intensity. We find that the Au_8–Au_8 dimer

has a higher density of states (DOS) than Au_8 by comparing their DOS in Fig. S4; this is consistent with the fact that more electrons are excited in the Au_8–Au_8 dimer. Additionally, the number of electron transitions from all occupied states to unoccupied states in both Au_8 and Au_8–Au_8 is higher at a higher intensity than that at a lower intensity.[33]

In summary, we have explored the nonlinear response induced by plasmons of gold nanoclusters using TDDFT. Our findings indicate that the third-order nonlinear effect is more pronounced in Au_8–Au_8 dimers than in individual Au_8 clusters. This can be attributed to the fact that in Au_8–Au_8 dimers a larger number of electrons transition from occupied to unoccupied states compared with in single Au_8 clusters. Furthermore, our results reveal the underlying microscopic mechanism by which the contribution of hot electrons generated by plasmon decay influences nonlinear responses. This finding is essential to elucidate the microscopic mechanisms and realize accurate regulation and control of nonlinear optics at the atomic level. Since the algorithm is limited at present, we do not calculate higher-harmonic generation, and we will study the higher-harmonic generation by changing the software algorithm in the future.

Acknowledgements

Project supported by the National Key R&D Program of China (Grant Nos. 2020YFA0211300 and 2021YFA1201500), the National Natural Science Foundation of China (Grant Nos. U22A6005, 92150110, 12074237, and 12304426), the Natural Science Foundation of Shaanxi Province (Grant No. 2024JC-JCQN-07), the Fundamental Science Foundation of Shaanxi (Grant No. 22JSZ010), and the Fundamental Research Funds for Central Universities (Grant Nos. GK202201012 and GK202308001).

References

[1] Xiao S, Qin M, Duan J, Wu F and Liu T 2022 *Phys. Rev. B* **105** 195440
[2] Koulouklidis A D, Gollner C, Shumakova V, Fedorov V Y, Pugzlys A, Baltuska A and Tzortzakis S 2020 *Nat. Commun.* **11** 292
[3] Ono M, Hata M, Tsunekawa M, Nozaki K, Sumikura H, Chiba H and Notomi M 2019 *Nat. Photon.* **14** 37
[4] Hafez H A, Chai X, Ibrahim A, Mondal S, Férachou D, Ropagnol X and Ozaki T 2016 *J. Opt.* **18** 093004
[5] Nitiss E, Hu J, Stroganov A and Brès C S 2022 *Nat. Photon.* **16** 134
[6] Provazza J, Tempelaar R and Coker D F 2021 *J. Chem. Phys.* **155** 014108
[7] Dai Y, Wang Y, Das S, Xue H, Bai X, Hulkko E, Zhang G, Yang X, Dai Q and Sun Z 2020 *ACS Nano* **14** 8442
[8] Li G C, Lei D Y, Qiu M, Jin W, Lan S and Zayats A V 2021 *Nat. Commun.* **12** 4326
[9] Li Y, Song Y, Zhang X, Liu T, Xu T, Wang H, Jiang D E and Jin R 2022 *J. Am. Chem. Soc.* **144** 12381
[10] Lien M B, Kim J Y, Han M G, Chang Y C, Chang Y C, Ferguson H J, Zhu Y, Herzing A A, Schotland J C, Kotov N A and Norris T B 2017 *ACS Nano* **11** 5925
[11] Singh D J, Krakauer H, Haas C and Liu A Y 1992 *Phys. Rev. B* **46** 13065
[12] Kauranen M and Zayats A V 2012 *Nat. Photon.* **6** 737
[13] Frischwasser K, Cohen K, Tsesses S, Dolev S, Rosenblatt G and Bartal G 2022 *Phys. Rev. Lett.* **128** 103901
[14] Marinica D C, Kazansky A K, Nordlander P, Aizpurua J and Borisov A G 2012 *Nano Lett.* **12** 1333
[15] Bonafé F P, Aradi B, Guan M, Douglas-Gallardo O A, Lian C, Meng S, Frauenheim T and Sánchez C G 2017 *Nanoscale* **9** 12391
[16] Choi Y M, Roh S H, Kwak E, Choi D-G, Kwon S J, Kim J K and Park J H 2023 *Chem. Eng. J.* **461** 142082
[17] Frontiera R R, Henry A I, Gruenke N L and Van Duyne R P 2011 *J. Phys. Chem. Lett.* **2** 1199
[18] Lin X R, You L X, He Q L, Zhuang W, Huang B Z and Zheng D X 2023 *Electroanalysis* **35** e202300001
[19] Gao S 2015 *J. Chem. Phys.* **142** 234701
[20] Ponkratova E, Ageev E, Komissarenko F, Koromyslov S, Kudryashov D, Mukhin I, Veiko V, Kuchmizhak A and Zuev D 2021 *Photonics* **8** 121
[21] Chen Q, Chen W, Miao B and Fan J 2022 *J. Am. Ceram. Soc.* **105** 4784
[22] Zhang Y, Grady N K, Ayala-Orozco C and Halas N J 2011 *Nano Lett.* **11** 5519
[23] Hanke T, Cesar J, Knittel V, Trugler A, Hohenester U, Leitenstorfer A and Bratschitsch R 2012 *Nano Lett.* **12** 992
[24] Goulielmakis E and Brabec T 2022 *Nat. Photon.* **16** 411
[25] Castro A, Appel H, Oliveira M, Rozzi C A, Andrade X, Lorenzen F, Marques M A L, Gross E K U and Rubio A 2006 *Phys. Stat. Sol. (b)* **243** 2465
[26] Ceperley D M and Alder B J 1980 *Phys. Rev. Lett.* **45** 566
[27] Troullier N and Martins J L 1991 *Phys. Rev. B* **43** 1993
[28] Sorensen C M and Fischbach D J 2000 *Opt. Commun.* **173** 145
[29] Yan L, Guan M and Meng S 2018 *Nanoscale* **10** 8600
[30] Li C, Lu X, Srivastava A, Storm S D, Gelfand R, Pelton M, Sukharev M and Harutyunyan H 2021 *Nano Lett.* **21** 1599
[31] Ma J, Wang Z and Wang L W 2015 *Nat. Commun.* **6** 10107
[32] Townsend E and Bryant G W 2014 *J. Opt.* **16** 114022
[33] Guan M, Yan L, Hu S, Zhang Y, Chen D and Meng S 2023 *Phys. Rev. B* **107** 075426